Dielectric and Magnetic behaviour of Substituted Strontium M-Hexagonal Ferrite

A THESIS SUBMITTED IN PARTIAL FULFILLMENT OF

THE REQUIREMENTS FOR THE DEGREE OF

BACHELOR OF TECHNOLOGY

By

SWAYAM MAJHI

Roll no:- 109CR0010

DEPARTMENT OF CERAMIC ENGINEERING

NATIONAL INSTITUTE OF TECHNOLOGY

ROURKELA

2012-2013

Dielectric and Magnetic behaviour of Substituted Strontium M-Hexagonal Ferrite

A THESIS SUBMITTED IN PARTIAL FULFILLMENT OF

THE REQUIREMENTS FOR THE DEGREE OF

BACHELOR OF TECHNOLOGY

By

SWAYAM MAJHI

Roll No:- 109CR0010

UNDER THE GUIDANCE OF

DR. JAPES BERA

DEPARTMENT OF CERAMIC ENGINEERING

NATIONAL INSTITUTE OF TECHNOLOGY

ROURKELA

2012-2013

NATIONAL INSTITUTE OF TECHNOLOGY
ROURKELA

CERTIFICATE

This is to certify that the thesis entitled, “Dielectric and Magnetic behaviour of Substituted Strontium M-Hexagonal Ferrite” submitted by Swayam Majhi in partial fulfilment of the requirements of the award of Bachelor of Technology Degree in Ceramic Engineering at National Institute Of Technology, Rourkela is an authentic work carried out by him under my supervision and guidance.

To the best of my knowledge, the matter embodied in the thesis has not been submitted to any other university / institute for the award of any Degree or Diploma.

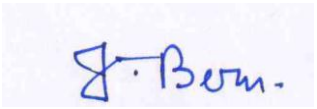

Date:

Dr. Japes Bera
(Associate Professor)
Dept. of Ceramic Engineering
National Institute of Technology
Rourkela-769008

Acknowledgement

I wish to express my deep sense of respect and regard for Prof. Japes Bera, Department of Ceramic Engineering, N.I.T Rourkela for introducing the research topic and for his inspiring guidance, constructive criticism and valuable suggestions throughout this research work. I would also like to thank him for his constant support and words of encouragement without which it would not have been possible for me to complete this research work.

I am also grateful to all the faculty members of the Dept. of Ceramic Engineering, whose immense knowledge in the field of ceramics has enlightened me in various areas of my research work.

I am also grateful to Mr Ganesh Kumar Sahoo, Miss Geetanjali Parida and all the other research scholars in the Dept. of Ceramic Engineering for their unparalleled help and support.

I am also thankful to Mr Prashant Mohanty, Mr Sushil Sahoo and all the other office staff for all their help. I would also like to thank my friends for all their suggestions and inputs for the betterment of my research work.

Finally, I deeply thank my parents for all their support and faith in me.

SWAYAM MAJHI
Roll No:- 109CR0010
B.Tech, Dept. of Ceramic Engineering
N.I.T Rourkela

Date:

ABSTRACT

$SrFe_{12}O_{19}$ is an important magnetic hexa-ferrite which is used for high frequency application in multilayer chip inductor. Generally $BaFe_{12}O_{19}$ is used for such high frequency applications but it has been observed that $SrFe_{12}O_{19}$ has better magnetic properties than the prior at high frequency range. This project concentrates on the preparation of $SrFe_{12}O_{19}$ samples along with other samples with substitution of Zn and Ti in the base composition and to study the changes in magnetic property due to these substitutions. All the products were synthesized via auto-combustion process. All the samples were characterized for their phase formation using XRD. The powders obtained by auto-combustion process were calcinated at 900^{o}c and then pressed into pellets and toroid samples. A dilatometry test was also carried out for bar shaped rectangular samples. These pellet and toroid samples were sintered at various temperatures. After sintering, these samples were characterized for their microstructural development, dielectric and magnetic properties. The dielectric and inductive property measurements were carried out by the help of a LCR meter. It has been observed that on introduction of Zn and Ti in $SrFe_{12}O_{19}$ and also the use of sintering additives like CuO gives better dielectric and magnetic properties than the undoped sample.

List of figures

List of tables

Contents

CHAPTER 1

INTRODUCTION

Introduction

In recent decades, there is a constant demand for signal processing devices in mobile communication, radar, satellite, security and defence, aerospace and automotive. Moreover, the operating frequencies of these devices are constantly shifting to higher values from microwave (0.3 to 100 GHz) to millimeter wave, which requires the use of high frequency material hexagonal ferrite [1].

The group of ferrites having hexagonal crystal structures is called hexagonal ferrite or hexa-ferrite. There are numbers of hexa-ferrite compound in the general composition $BaO\text{-}MeO\text{-}Fe_2O_3$, where Me is a small 2+ ion such as cobalt, nickel or zinc, and Ba can be substituted by Sr. Important types of hexa-ferrites are designated as M, W, Y, Z, X and U types. The chemical formulas of them are:

- M-type: $BaFe_{12}O_{19}$ (BaM) or $SrFe_{12}O_{19}$ (SrM),
- W-type: $BaMe_2Fe_{16}O_{27}$,
- Y-type: $Ba_2Me_2Fe_{12}O_{22}$,
- Z-type: $Ba_3Me_2Fe_{24}O_{41}$,
- X-type: $Ba_2Me_2Fe_{28}O_{46}$
- U-type: $Ba_4Me_2Fe_{36}O_{60}$.

They are all ferrimagnetic materials and their magnetic properties are intrinsically linked to their crystal structure. All have magneto-crystalline anisotropy (MCA) that is the induced magnetisation has a preferred orientation within the crystal structure. On the basis of MCA, they can be divided into two main groups, those with

(1) Easy axis of magnetisation, the **uniaxial** hexaferrites and

(2) Easy plane (or cone) of magnetisation, known as **hexaplana** ferrites.

M, Z, W, X and U-types ferrites are uniaxial and Y-type is hexaplana ferrites. However, Co_2Z, Co_2W, Co_2X and Co_2U ferrites have planar anisotropy [2].

The compound with greatest technological interest is M-hexagonal ferrites. They are magnetically very hard materials due to their uniaxial and high MCA constants. Their magnetisation is locked rigidly along the preferred *c*-axis of the hexagonal structure. The high MCA is prerequisite for a high coercivity, which results a magnetically hard material suitable for permanent magnets [1]. On the other hand, hexaplana ferrites have a preferred direction of magnetization either in the hexagonal basal plane or in a cone and they are excellent soft magnet due to free rotation of magnetisation in the plane/cone. It has been reported that ferrites with planar MCA exhibit good magnetic performance in the GHz range and have higher resonance frequency compared to spinel ferrites [1]. To make them more useful in high frequency GHz application, M-ferrites are substituted with different cations (for example, Co^{2+} and Ti^{4+} for Fe^{3+}), which changes its MCA from uniaxial to planar type.

For high frequency application, the MW dielectric losses of ferrites must be minimized. The dielectric losses due to the damping of the vibration of electrical dipoles, dominate at higher frequencies, causing a high decrease of permittivity in most materials. For that reason, ferrites must have good electrical insulation and moderate permittivity to allow the full penetration of electrical field. Most hexagonal ferrites are better than cubic spinel ferrite with respect to above two properties and therefore are well suited for high frequency applications.

In addition to the high operating frequency, current generation electronic devices are becoming smaller with less weight and more efficient day by day. For that, the passive components are used in the form of multilayer chip component and are

surface mounted on printed circuit boards. The recent trend is the integration of different passive components onto a single Si-wafer platform enabling more reduction of device volume and weight. For both the technologies, low temperature co-fired ceramics (LTCC) is required for co-sintering with internal metal electrode. One of such component is multilayer ferrite chip inductor (MLFCI) shown in Fig.1.

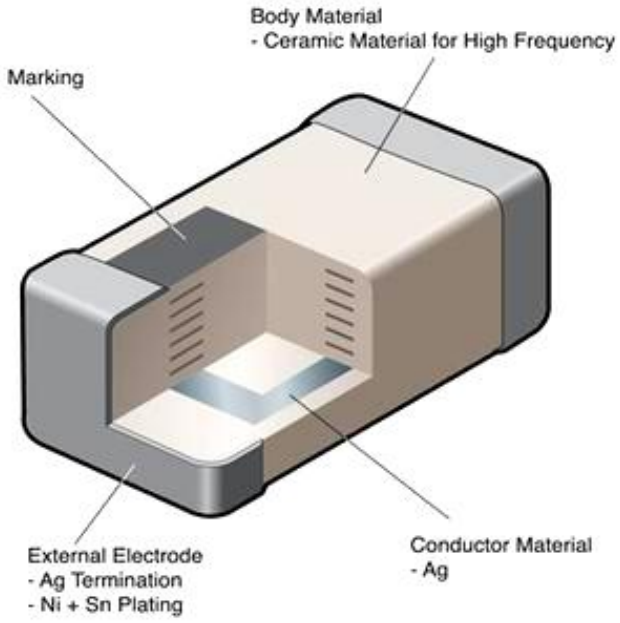

Fig. 1. Multilayer ferrite chip inductor (MLFCI).

Many of the MLFCI are made of soft ferrite materials like nickel-copper-zinc ferrite, with their operating frequencies in lower MHz range (Fig. 2(a)). NiCuZn ferrite is not suitable at MW/GHz frequency due to low self-resonance frequency (SRF). The SRF is the frequency above which μ_{eff} falls very rapidly due to spin relaxation, domain wall resonance, etc. The resonance can be seen from the Fig. 2 where the real permeability (μ') and imaginary permeability (μ'') components of the complex permeability for NiCuZn [3] and BaM ferrites [4] are plotted with frequency. SRF is defined as the point at which μ'' is maximum and that also coincides with the half value of μ' peak. The SRF (f_r) is inversely proportional to the initial permeability (μ_i) as per the relation;

$$f_r = (0.1\gamma M_s)/\mu_i \qquad (1.1)$$

where, γ is the ratio of the magnetic moment to torque for an electron, called gyromagnetic ratio, $M_s$is the saturation magnetization.

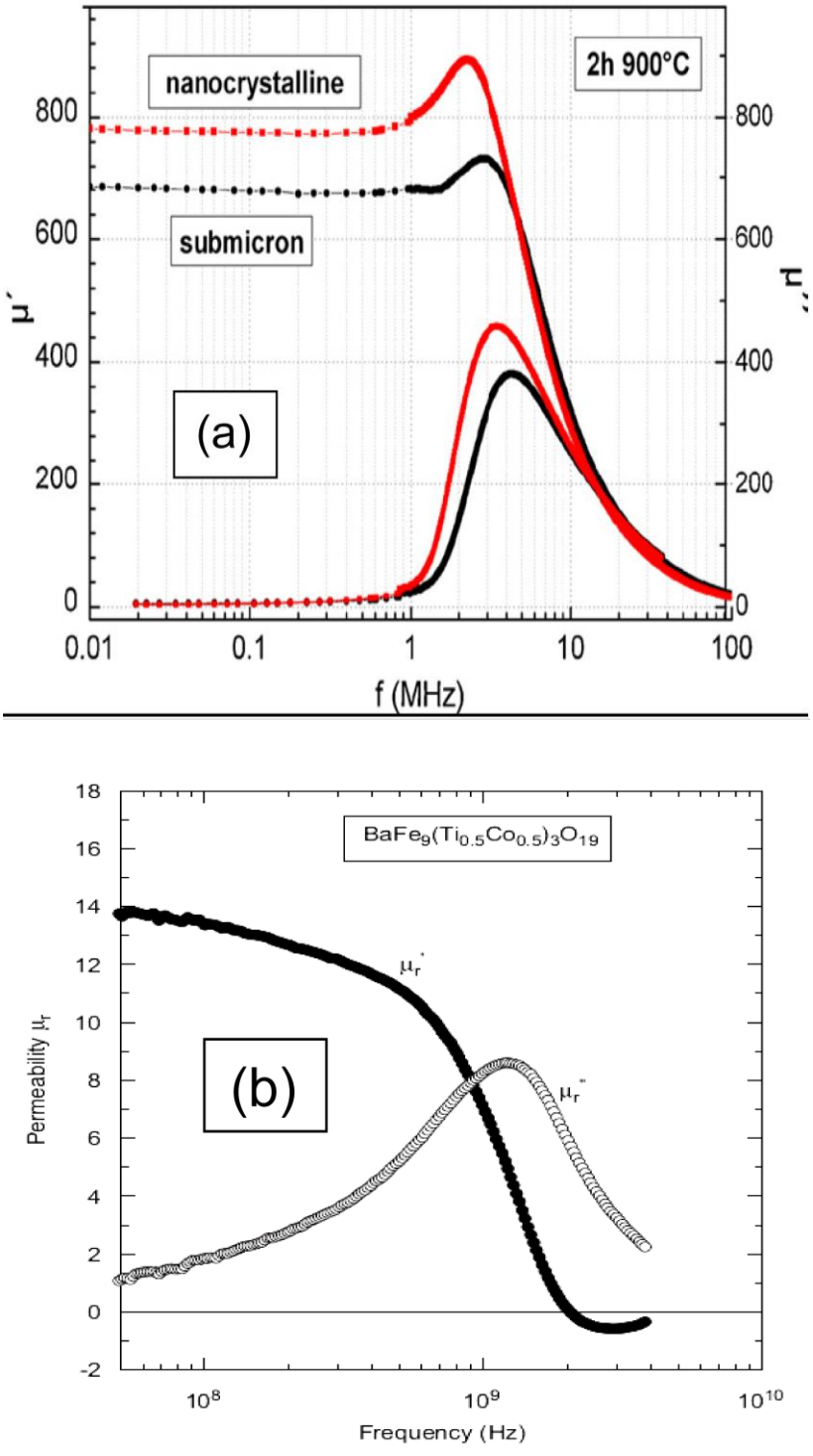

Fig. 2. Real (μ') and imaginary permeability (μ'') component of the complex permeability of, (a) NiCuZn ferrites prepared from nanocrystalline and submicron-size powders [3], and (b) $BaFe_9(Ti_{0.5}Co_{0.5})_3O_{19}$ ferrite [4].

NiCuZn ferrite has SRF in the range of few MHz (~1-3) due to its high initial permeability (~900). Most hexaferrites do not have this frequency limitation as they have SRF in GHz range due to low permeability (~20). For example, $BaFe_{9.6}Co_{1.2}Ti_{1.2}O_{19}$ ferrite has SRF of 1.2 GHz [6] as shown in Fig. 2(b). The SRF (f_r) also related to the anisotropy;

$$f_r = (\gamma/2\pi)\, H_a \qquad (1.2)$$

where, H_a is the magnetic anisotropy field, which express the degree of MCA. Ba-M ferrite has high $H_a$value of 17000 Oe [2] compared to low value 198 Oe for NiCuZn ferrite [1]. This high anisotropy field produces a GHz range SRF for BaM-ferrites. In fact, BaMhexaferrite has been proposed for high frequency chip application in a recent US patent [5]. SrM ferrite can be another material for high frequency application as it has slightly better magnetic properties than those of BaM [2] as shown in Table 1.

Table 1.Comparison of magnetic properties of BaM and SrM ferrites [2].M_s is saturation magnetization, H_a is magnetic anisotropy field, K_1 is magnetic anisotropy constants, and T_c is Curie temperature.

Ferrite	Formula	M_s (A m^2 kg^{-1})	H_a (kA m^{-1})	K_1 (erg/cm^3)	T_c (^oC)
BaM	$BaFe_{12}O_{19}$	72	1353	$3.3x10^6$	450
SrM	$SrFe_{12}O_{19}$	92-74	1592	$3.5x10^6$	460

For the fabrication of MLFCI, ferrite is co-sintered with an internal metal. The structure and manufacturing process of MLFCI is shown in Fig.3. Silver (Ag) is usually most suitable internal electrode as it has;

- High conductivity
- Lower cost
- Lower electrical losses.

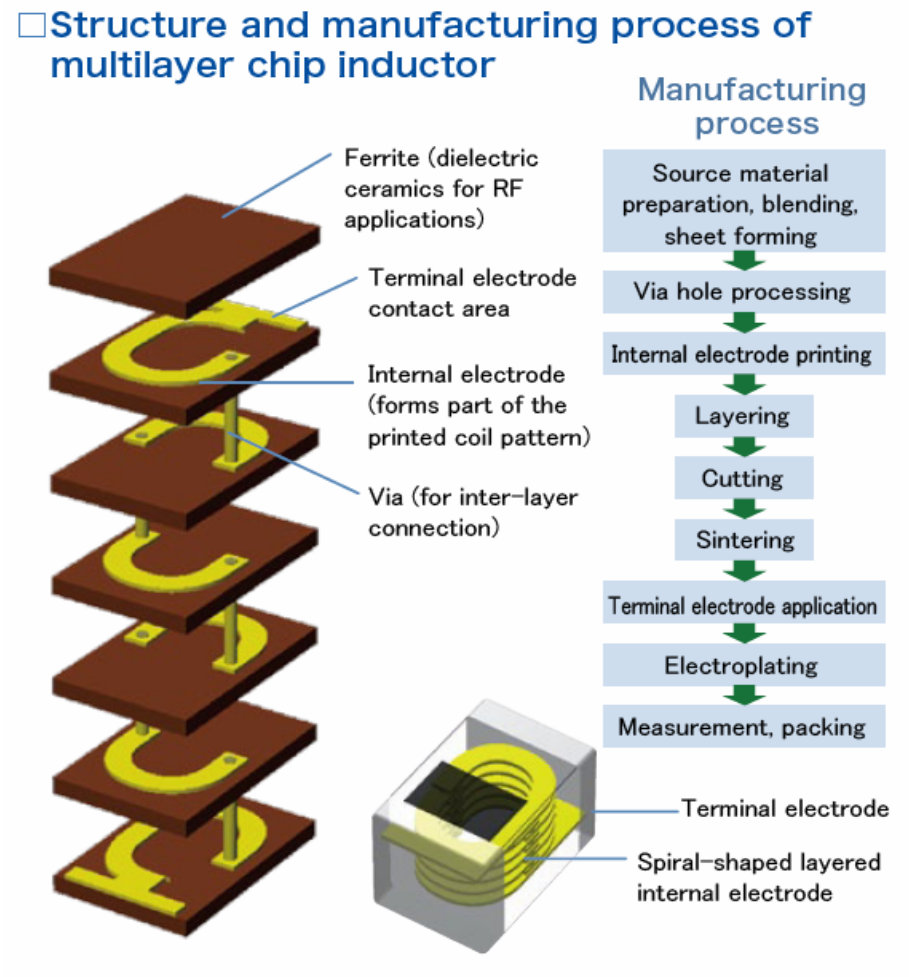

Fig. 3. The structure and manufacturing process of MLFCI [6].

As silver melts at 961^{o} C, the ferrite composition must be co-sintered at a temperature sufficiently lower than that, preferably at 900^{o} C, to prevent possible diffusion of Ag into the ferrite. Otherwise the diffusion of Ag metal may decrease the permeability of the ferrite. For low temperature sintering of the ferrites, usually sintering additives like glass, Bi_2O_3, are used. However, the sintering additive decreases the permeability of ferrite, and the quantity of additive should be as low as possible. Additionally, sinter-active fine ferrite powders are used for chip fabrication. Another solution could be a suitable modification of the ferrite composition enabling its low temperature

sintering. As mentioned above, a recent patent [5] discloses such a modified composition of BaM ferrite which is capable of being sintered at 920^{o} C without the use of any sintering additive.

Substituted Z and Y-type hexaplana ferrites are also used for GHz applications. However, they are not so compatible with the LTCC multilayer technology. Their synthesis requires high temperatures which contradicts the required low-temperature sintering behaviour of MLFCI [7]. CoZnCu-Z and CoZnCu-Y ferrites were suggested as promising high frequency materials [8, 9]. However, they were sintered at 1300^{o} C for Z ferrite and 1000-1100^{o} C for Y ferrites. Nevertheless, the synthesis of single phase and thermally stable Z and Y ferrites are very difficult. Substituted Y-ferrites are thermodynamically not stable below 950^{o} C [10] and Z-ferrites frequently decompose to a mixture of Z-, Y-, and M-type ferrites during sintering even at 900^{o} C [11]. On the contrary, Co/Ti substituted BaM ferrites are reported to be thermally stable during co-firing at 900^{o} C and have been proposed as an excellent magnetic material for MLFCI [7]. In this case, a low temperature glass sintering aid was used to produce a dense ferrite with a permeability of μ'=13 and SRF of 1 GHz.

With this background, it may be concluded that SrM ferrite will be a good candidate for high frequency chip application with respect to the enhancement of SRF. As stated above, SrM ferrite has higher saturation magnetization and magnetic anisotropy field H_a than BaM ferrite and expected to show better high frequency properties compared to BaM ferrite.

CHAPTER 2

LITERATURE REVIEW

Introduction:

In this section an effort has been made to provide a detailed review of the research work undertaken by various researchers on the synthesis of $SrFe_{12}O_{19}$ and the effect of doping of various divalent cations on the magnetic and electric property as well as the effect of various sintering additives on the sintering temperature.

Many research works have been carried out to improve the elecro-magnetic properties of $SrFe_{12}O_{19}$. One of these attempts is by the substitution of various divalent cations like Co ,Ti , Zn, La (trivalent) in $SrFe_{12}O_{19}$.

The Sr-M ferrites have been synthesized through different routes like; conventional solid oxide reaction [12], co-precipitation [13], sol-gel [14], hydrothermal [15], glass crystallization [16], combustion method [17], etc. The phase formation of these hexaferrites is an extremely complicated process and their formation mechanisms are not yet fully understood [2]. SrM has been synthesised through conventional solid oxide reaction by calcining oxide raw materials at 1000^{o} C for 12 h [12]. However, the phase can be synthesized at a temperature as low as 700^{o} C by sol-gel processing [14]. So the sol-gel processing could be an effective route for the synthesis of fine-grained sinter-active ferrite powders.

Magnetic properties of the ferrite depend on many parameters like density, grain size, chemical composition and grain alignment. In general, higher is the density higher will be saturation magnetization (M_s) and lower the grain size higher will be coercive field (H_c). The cation substitution is one of the most important methods for improving magnetic properties of ferrites. M_s of the ferrite can be increased by the substitution of non-magnetic Zn^{2+} for Fe^{3+}, where Zn^{2+} prefers tetrahedral positions of

the crystal structure. The substitution reduces the negative contribution of tetrahedral-octahedral anti-ferromagnetic coupling. Other 2-valence cations like Cu, Ni, Co, Mg and Mn have also been substituted for Fe^{3+}. The charge compensation for these substitutions is done either by substituting Ba with 3-valence cation or by substituting Fe with 4-valence cation. Different 3-valance cations like V, Ga, Al, In or Sc and 4-valance cations like Ti, Sn, Zr, Hf, Ce or Ru have been substituted in the ferrite [2].

The most common substitution in M-ferrite is $BaCo_xTi_xFe_{12-2x}O_{19}$ and the substitution is very important for tailoring anisotropy and microwave properties of M-ferrite [2]. With the increase in *x*, grain size, M_s *and* H_c decreases. Ti plays major role in decreasing grain size and Co plays role in the change of magnetic properties. The axial anisotropy of the ferrite decreases with the substitution and converted into in-plane anisotropy. Hence, a very soft ferrite can be achieved with the substitution while keeping $M_s$value reasonably stable. Other major advantage of Co^{+2}/Ti^{+4} substitutions is increased resistivity of the substituted ferrite. Similar behavior is found in other substitutions like; CoZr-*M*, CoSn-*M*, NiZnTi-*M*.

It has been found that a stoichiometric mixture of ferrite powders never sinter fully, whereas Fe deficient material can be fully densified. This is attributed to increased diffusion rates in the non-stoichiometric mixes due to induced lattice defects. For co-sintering with Ag internal electrode in a MLFCI, the sintering temperature of ferrite must be reduced to 900^o C or less. Two most effective approaches to reduce the sintering temperature are (1) Use of additives like glass, Bi_2O_3,B_2O_3, SiO_2, for liquid phase sintering and (2) Partial substitution of metal cations by Cu or addition of CuO. There are only few reports on reduction of sintering temperature of Sr-M ferrite by CuO addition [18, 19]. The major mechanism proposed [12] for enhanced sintering

was the formation of Cu-rich eutectic phase which melts below 1000^{o} C and enabled the reactive liquid-phase sintering of CuO added SrM ferrite. They also proposed that Cu^{2+} was not substituted in hexagonal structure, rather spinel type Cu-ferrite and Cu-rich eutectic phases were formed.

There are very few international patents on this typical issue. The patent on "Ferrite Material for a Permanent Magnet and Method for Production There of" [18], disclosed about low temperature sintered Sr-M ferrite for MLFI application. However, one recent patent [5] discloses about the composition based on the low temperature sintered Ba-M ferrite for chip bead and antenna application in few 500 MHz frequency band. There are no Indian patents available related to this specific subjects.

WandeeOnreabroyet. al. [20] investigated the structural and magnetic properties of $Sr_{0.8}La_{0.2}Fe_{12}O_{19}$ which were fabricated by conventional ceramic process. It was observed by studying the XRD patterns that the undoped sample had a hematite phase which was much lower in case of the doped specimen. By SEM analysis it was also observed that by the doping of La^{+3} caused a lesser increase in average grain size as compared to the undoped specimen. The study also showed that the doped sample had higher values of saturation magnetization than before.

Ali Ghasemiet. al. [21] prepared Sn and Zn substituted Strontium hexa-ferrite by a sol-gel process onthermallyoxidizedsiliconwafer (Si/SiO2). The SEM analysis of samples showed that on increasing Sn-Zn content the grain size decreased. It was also observed that by increasing the substitution content in the ferrite thin films, the coercivity value and saturation magnetization values increased but magnetic interaction reduced.

QingqingFanget. al. [22] prepared strontium hexa-ferrite nanoparticles through a chemical sol-gel process. The strontium hexa-ferrite was substituted by Zn^{+2}, Ti^{+4}, Ir^{+4} and it was observed that (Zn, Ti)$_x$ shows higher values of both coercivefield strength and saturation magnetization than the (Zn, Ir)$_x$ substituted phase for $0 < x \leq 0.6$.

XiansongLiuet. al. [23] synthesized strontium hexa-ferrite by ceramic process where $Sr^{+2}$was substituted by La^{+3} and Fe^{+3} was substituted by Co^{+2} according to the formula $Sr_{1-x}La_xFe_{12-x}Co_xO_{19}$. It was observed that when an appropriate amount of substitution of $La^{+3}$and Co^{+2} was done then an increase in saturation magnetisation and intrinsic coercivity resulted.

Ali Ghasemi[24] prepared $SrFe_{12-x}(Zr_{0.5}Mg_{0.5})_xO_{19}$ by sol-gel method where x = 0 to 2.5. The magnetic properties of this sample was studied with the help of a vibrating sample magnetometer (VSM) and it was observed that with an increase in Zr-Mg substitution content the coercivity decreases but saturation magnetisation value increases.

Kubo et. al. [25] invented a composite type magnetic particles (A) each of which contains hexagonal ferrite and spinel structure ferrite and single phase type magnetic particles of hexagonal ferrite (B). This type of magnetic particle has a stronger resistance to noise than that made by using single phase type magnetic particles of hexagonal ferrite thereby providing excellent electromagnetic characteristics. This also provides a higher signal to noise ratio for short wavelength range. The formula for the compound is $AO_n(Fe_{12-x-y}M(1)_xM(2)_yO_{18-z})$ where A = Ba / Sr / Ca / Pb , M(1) = Co / Zn / Ni / Cu / Mn / Fe, M(2) = Ti / Sn / Ge / Zr / Sb / Nb / V / Ta / W / Mo. X can vary from 0.5 to 0.3 , Y from 0 to 2.0 and Z can be 0.05 or larger. When A : B = 5

: 95 to 30 : 70 it can be used as a magnetic recording medium for 1μm wavelength or lower and when A : B = 70 : 30 to 95 : 5 it can be used for 1μm wavelength or higher.

Objective of the project

1) First objective is to prepare sinter-active powder of Zn and Ti substituted $SrFe_{12}O_{19}$ M-hexagonal ferrite through sol-gel combustion method.

2) Second objective is to add CuO and Bi_2O_3 sintering additives to decrease the sintering temperature below 1000^oC.

CHAPTER 3

EXPERIMENTAL PROCEDURE

3.1 Synthesis of Strontium M-Ferrite Powder

The strontium M-ferrite powder were synthesized by sol-gel auto combustion method. Strontium nitrate [$Sr(NO_3)_2$], Iron nitrate [$Fe(NO_3)_3$], Zinc nitrate [$Zn(NO_3)_2.6H_2O$], Titanium oxide [TiO_2], Copper nitrate [$Cu(NO_3)_2.3H_2O$] , Bismuth oxide [Bi_2O_3] and Citric Acid [$C_6H_8O_7$] were used as precursors for the fabrication of the powder by auto combustion method. All the chemical used were of analytical grade with 99.8% purity.

3.1.1 Sol-gel auto combustion synthesis

Pure and substituted $SrFe_{12}O_{19}$ (SrM) powders were synthesized by sol-gel auto combustion process. This process is preferred because it has advantages such as low external energy consumption, simple equipment requirement, simple preparation method and inexpensive precursors which give homogeneous, nano-sized, highly reactive powders [26]. The auto combustion synthesis process also known as self-propagating synthesis was first developed in Russia by Merzhanov and had been used successfully in preparation of complex oxides like ferrites and high temperature superconductors [27].

Auto-combustion synthesis route involves exothermic redox reaction between organic fuel and a metal nitrate to yield multi-element oxide. In contrast to a high temperature furnace, the auto-combustion synthesis is self-sufficient to provide the energy required for the reaction to take place. The organic fuel along with metal nitrates is mixed with distilled water to form an aqueous solution which maximizes the molecular mixing of the constituent components. This solution is then slowly heated to dry it and ultimately transform it to a gel.

Due to constant supply of heat the gel eventually ignites in a self-propagating combustion manner until all the gel is completely burnt out. This self-propagating combustion reaction lasts about 2-5 seconds to yield the desired product. This route yields a highly homogeneous product in a very short period of time which does not require the usage of expensive high temperature furnaces. The parameters that influence an auto-combustion synthesis reaction are fuel to oxidizer ratio (f/o), ignition temperature, water content of the precursor mixture and the type of fuel used. The fuel to oxidizer ratio is critical from the reaction point of view. The flame temperature of the reaction can be controlled by varying ratio of fuel to oxidizer.

The elemental stoichiometric coefficient, ϕ_e, is used to control the ratio of fuel to oxidizer in the reaction and is expressed as [28]:

$$\phi_e = \frac{\sum \text{Total valencies of oxidizing elements in the nitrates and fuel}}{(-1)\sum \text{Total valencies of reducing elements in the nitrates and fuel}} \quad (3.1)$$

Here ϕ_e is the ratio between oxidizing and reducing components of the metal- nitrate to the fuel mixture. The reaction is stoichiometric at the condition when $\phi_e = 1$. The metal-nitrate/fuel mixture is fuel rich if $\phi_e < 1$ and the mixture is fuel deficient or fuel lean and does not have enough fuel for the completion of the reaction when $\phi_e > 1$.

Fig 4 shows the flow diagram for auto-combustion synthesis of hexagonal M-ferrite powders. The M-type hexagonal ferrite powder was synthesized by an amount of 10 gms per batch. To prepare 5 gms batch of $SrFe_{12}O_{19}$ 4.7088×10^{-3} mol of Strontium nitrate, 0.056506 mol of Iron nitrate were taken. The total amount of metal ion present in the solution was 0.0612148 mol so equal mol of citric acid i.e. 0.0612148 mol of citric acid was added to the solution and the complete mixture was thoroughly mixed by stirring.

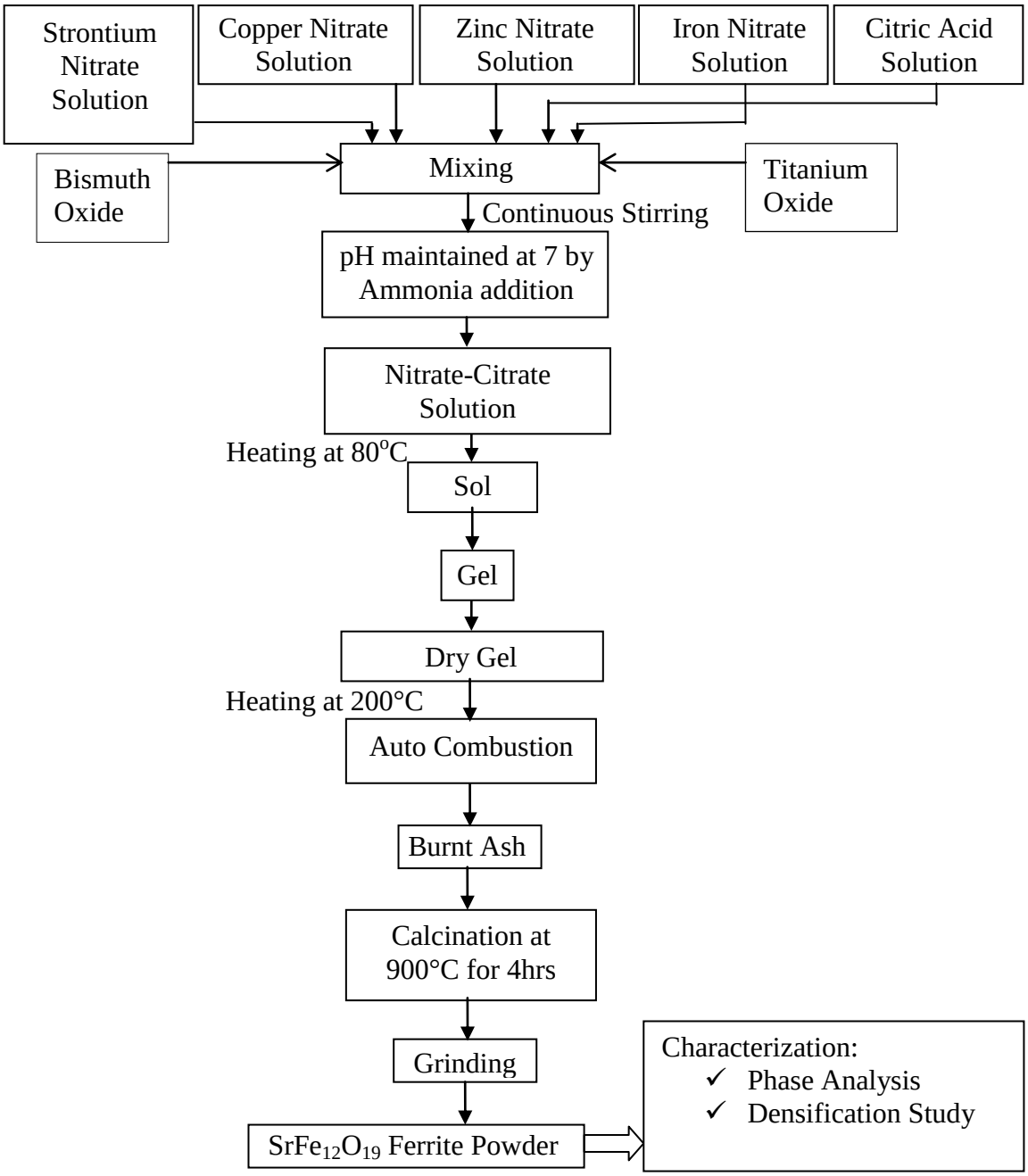

Fig. 4. Flow diagram for auto combustion synthesis of $SrFe_{12}O_{19}$ ferrite powder.

In Zn, Ti, CuO substituted $SrFe_{12}O_{19}$ as well as for addition of 1% Bi_2O_3 into $SrFe_{12}O_{19,}$ required moles of substituents was added to the solution before the addition of citric acid. The mixture thus obtained was placed in a beaker and was homogenized by continuous stirring. Then the pH of the solution was approximated to 7 by drop by

drop addition of ammonia solution. Then the solution was heated slowly on a hot plate at a temperature of 80^{o}C. This continuous slow heating gives rise to a sol which again converts to a gel. For the synthesis of Ti substituted $SrFe_{12}O_{19}$ Titanium dioxide was used.

The gel thus obtained was dried at 200^{o}C until the gel ignited in a self-propagating combustion manner to finally yield a fluffy structured material as shown in Fig. 5. This fluffy material was further ground to obtain hexagonal ferrite powder which was again calcined at 900^{o}c for 4 hours and finally ground to get hexagonal strontium M-ferrite powder.

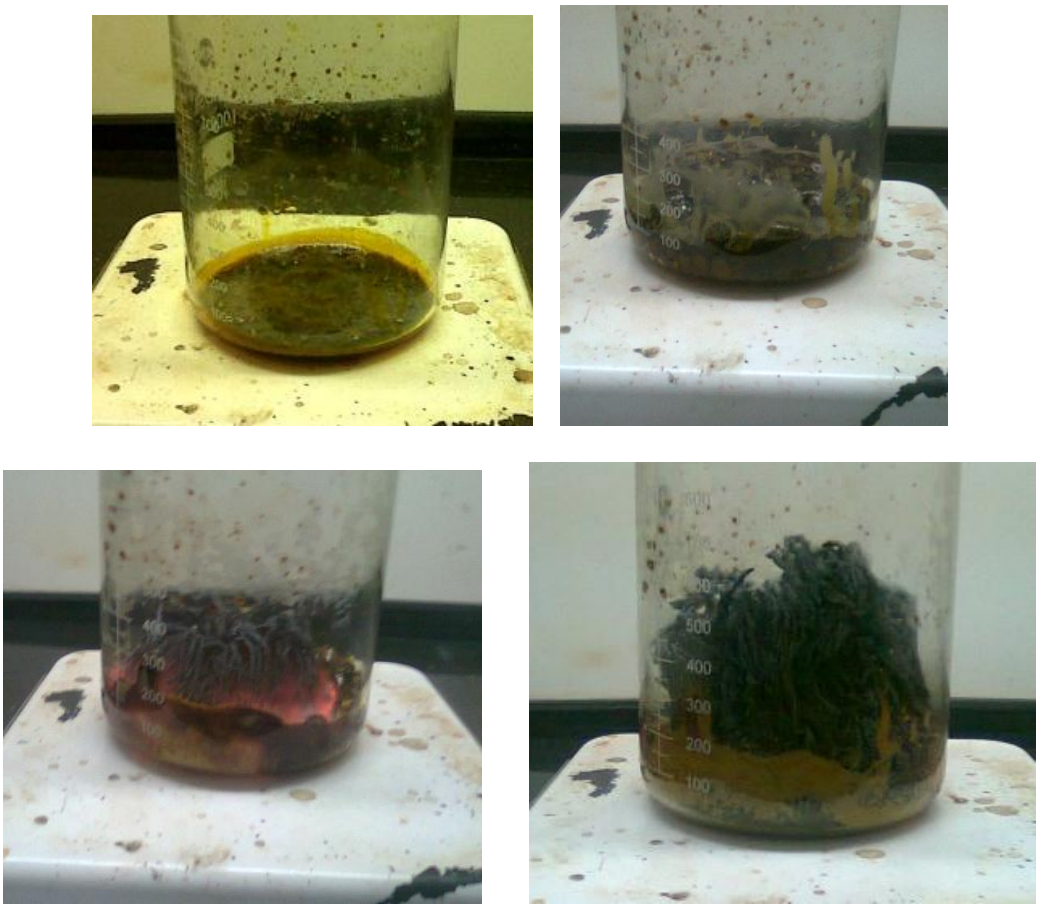

Fig. 5. Photographs of various stages of auto-combustion synthesis process

3.2 Dried gel and powder characterization

3.2.1 Phase Analysis

The phase formation characteristic of the burnt and calcined ash powder was studied by using powder X-ray Diffraction performed with the help of Philip's Diffractometer (model: PW-1830, Philips, Netherlands). For the detection of diffracted X-rays, there is an electronic detector on the other side of the sample in the X-ray tube. The sample is then rotated through different Bragg's angles. The track of the angle (θ) is kept with the help of a goniometer, the detector records the detected X-rays in counts/sec and sends this data to the computer. After the complete scan of the sample the X-ray intensity versus angle theta (2θ) is plotted. The angle (2θ) for each diffraction peak is then converted to *d*-spacing, using the Bragg's law; nλ= 2*d* Sinθ, where λ is the wave length of x-ray and n is order of diffraction. The phases that were present in the sample were identified by the help of Philips X-pert high score software.

The lattice parameter for hexagonal ferrite structure was determined using:

$$\frac{1}{d^2} = \frac{4}{3}\left(\frac{h^2+hk+k^2}{a^2}\right) + \frac{l^2}{c^2} \qquad (3.2)$$

Where '*a*' and '*c*' are lattice parameters,'*d*' is the d-spacing and (*hkl*) is miller indices.

3.2.2 Densification study

The densification kinetics of compact rectangular samples was done with the help of NETZSCH dilatometer model DIL 402 C. In the dilatometer the sample is placed in a sample holder which is situated in the centre of the furnace. The shrinkage or expansion characteristic of the sample is recorded by a push rod (pressed against the sample inside the furnace) which is connected to the measuring head. This experiment was carried out for different samples for temperature ranges like room temperature to 1100^{o}C, 1150^{o}C and 1200^{o}C at a rate of 10^{o}C per minute in an atmosphere of air.

3.3 Fabrication and sintering of ferrite parts

3.3.1 Fabrication

The powder of each batch which was earlier calcined at 900^{o}c for 4 hours was mixed with 5 wt% binder (polyvinyl alcohol). The following flow diagram (Fig. 6) shows the entire process.

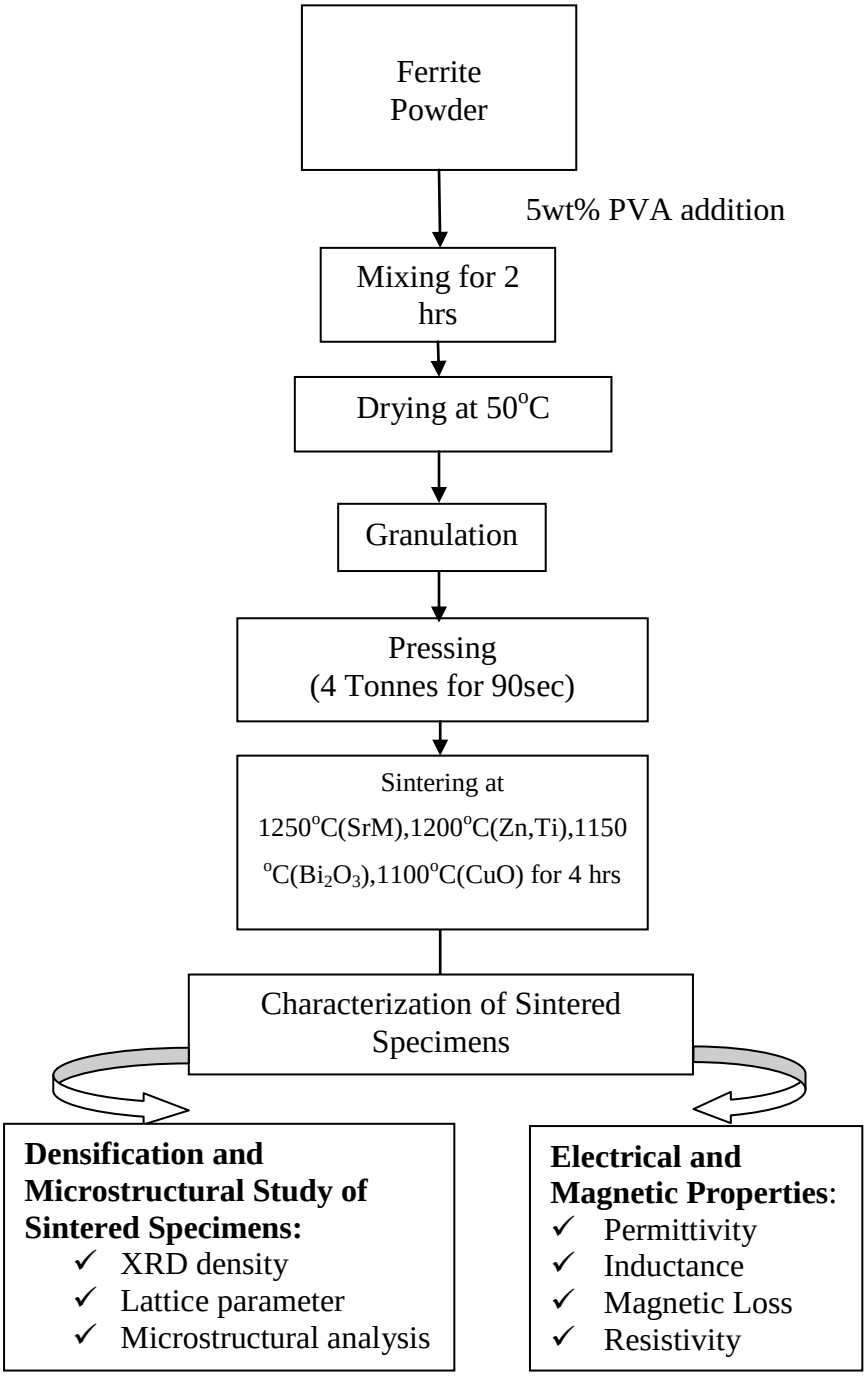

Fig. 6. A flow chart of fabrication and characterization for sintered ferrite parts.

Initially the calcined powders were mixed with 5 wt% PVA binder solution for about 2 hours and then dried at about 50^{o}C. Then the resulting specimen was granulated and then pressed in the form of pellets with diameter-15mm, and thickness- < 3mm using a uniaxial hydraulic press at a pressure of 4 Tonnes for 90 seconds.

3.3.2 Sintering

The uniaxially pressed pellet samples were sintered in an electric furnace at various temperatures: 1250^{o}C for $SrFe_{12}O_{19}$ (SrM) , 1200^{o}C for $SrFe_{11.6}Zn_{0.2}Ti_{0.2}O_{19}$(ZnTi-SrM), 1150^{o}C for 1% Bi_2O_3 added $SrFe_{11.6}Zn_{0.2}Ti_{0.2}O_{19}$ (Bi-doped)and 1100^{o}C for to $SrFe_{11.1}Cu_{0.5}Zn_{0.2}Ti_{0.2}O_{19}$ (CuO-doped).

The thermal regime of the furnace was controlled through a "Eurotherm" programmer-cum-controller within ± 2°C accuracy. The pellet samples were heated from room temperature to 650^{o}C at 1^{o}C/min followed by soaking at 650^{o}C for 2 hours and then heating at 3^{o}C/min till the sintering temperature and then soaking at the sintering temperature for 4 hours. Then the samples were cooled inside the furnace at 3^{o}C/min till room temperature was reached.

3.4 Characterization of Sintered Specimens

The physical properties of the sample such as microstructural analysis and phase analysis were done. The dielectric and magnetic properties were also characterized for torroids and sintered pellet samples.

3.4.1 Microstructural Analysis

The microstructures of the sintered pellets were studied with the help of Scanning Electron Microscopy (SEM). The SEM has an electron gun which under vacuum conditions emits a beam of electrons which is allowed to pass through a series of electromagnetic lenses before falling on the surface of the sample. The

voltage range of the electron beam is in the range of 1-30 kV. When the electron beam interacts with the surface of the sample a part of it is reflected as back scattered electron (BSE) and also as low energy secondary electron (SE), cathode luminescence, X-ray excitation beam and some part of the electron beam is transmitted.

The secondary electron beam forms an image which is studied in the extrinsic mode of SEM. These secondary electrons are then displayed on a television screen. The image thus formed would be bright if there is high secondary electron emission and this type of high emission is due to surface structure of the sample. The final picture which is obtained has brightness associated with surface characteristics and the image is normally illuminated. The samples were mounted on a metal stub with carbon paint. The mounted samples were studied by SEM (JEOL-JSM840).

3.4.2 Phase analysis

The phase analysis was done by using XRD technique. The details of this method have already been discussed in section

3.4.3 Dielectric characterization

For the dielectric characterization the sintered pellet samples were first cleaned with acetone and then a layer of silver paste was applied on the top and bottom surface of each pellet. Then these pellets were cured in a furnace at 650^{o}C for 30 mins. After curing the dielectric test of these samples was carried out.

The device used for this characterization was LCR HiTESTER (Model 3532-50) HIOKI. The measurements for this test were taken in the range of 100Hz to 1MHz. The graphs of tan δ vs frequency and permittivity vs frequency was plotted and analysed, where tan δ = dissipation or loss factor and relative permittivity is:

$$\acute{\varepsilon} = \frac{C \times d}{\ddot{\varepsilon} \times A} \qquad (3.5)$$

ε'' = relative permittivity of air (8.854 x 10^{-12} F m^{-1})

C = capacitance

d = thickness of pellet

A = area of the top surface of pellet.

3.4.4 Inductance and Magnetic Loss

Magnetic loss and inductance are the most primary magnetic characteristic property of any ferrite. The instrument that was used to measure this property was the LCR HiTESTER (Model 3532-50) HIOKI. This instrument has a maximum frequency limit of 5 MHz and was used to measure *tan* δ and inductance on toroid samples which were wound by low capacitive six turns of enamelled copper wire as shown in Fig. 7. The importance of this winding is that the stray capacitance (unwanted capacitance which can allow signals to leak between circuit wires) can be reduced by this special winding of the ferrite core [29].

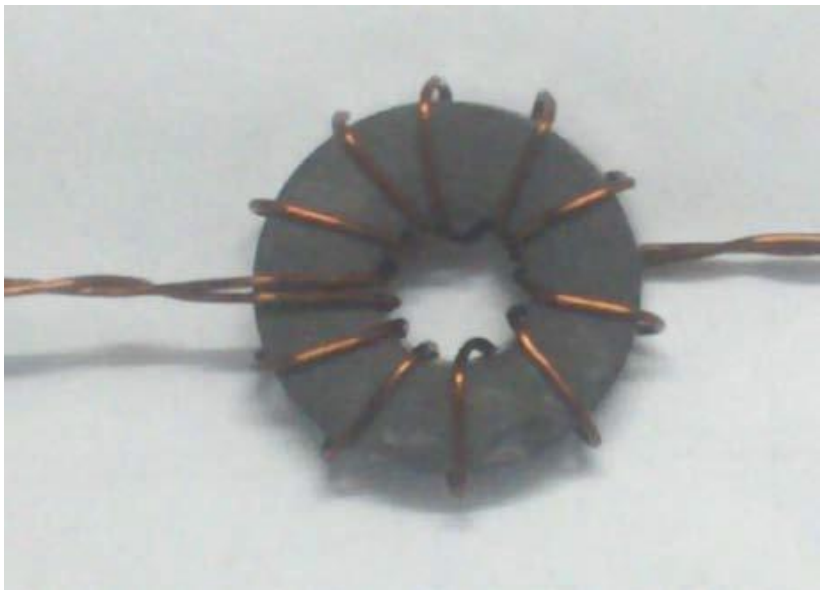

Fig. 7. Toroid sample with low capacitive six turn copper winding

The inductance of a ferrite core depends upon length of the coil, number of turns, diameter of the coils and the nature of the ferrite composition. Inductance is the ratio of the total magnetic flux linkage to the current (I) through the ferrite core. The total magnetic flux linkage depends on magnetic permeability (μ) of the medium or core material. This tells us that magnetic inductance is directly proportional to magnetic permeability. The initial permeability was calculated from the data of inductance by the use of the following formula:

$$\mu' = \frac{L}{2 \times 10^{-7} \times Na^2 \times H_t \times \ln[\frac{D_o}{D_{in}}]} \qquad (3.6)$$

Where L = inductance

N_a = number of turns

H_t = height of toroid

D_o = outer diameter of the toroid

D_{in} = inner diameter of the toroid

Many core losses which occur in cases of ferrites are due to hysteresis loss, eddy current losses and residual losses. The generation of hysteresis loss is due to irreversible rotation of magnetization vector. The eddy current loss is generated due to the current induced in the core under the influence of a time varying magnetic flux. The residual loss is caused by the power dissipation due to the reversible domain wall damping and the reversible rotation of domains. The relative loss factor (RLF) which is the ratio of *tan δ* (loss tangent) to *μ'* (initial permeability) was calculated.

3.4.6 Resistivity

The sintered hexagonal ferrite pellets were coated with conductive silver paste and cured at 650^{o}C for 30 mins. The AC resistivity ρ can be calculated as per the following formula [30]:

$$\rho = \frac{1}{\omega.\varepsilon o.k'.\tan\delta} = \frac{A}{2\Pi f.\tan\delta.C.t} \quad (3.7)$$

where, ε_0= permittivity of free space

k' = relative dielectric constant

tanδ = dissipation or loss factor

ω = angular frequency

C = capacitance

A and t are the area and thickness of the sintered pellet respectively.

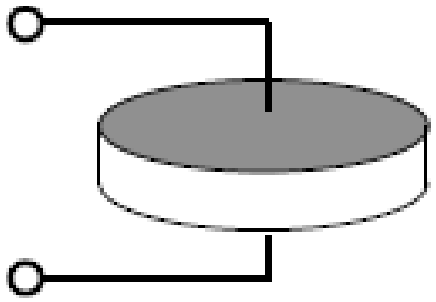

Fig. 8. Schematic electrode arrangement on the sintered pellet sample.

The Impedance Analyzer (Model 4192A, Hewlett Packard, USA)was used to measure the capacitance and tanδ on pellet sample. Variation in capacitance and tanδ with frequency was also measured and resistivity vs. frequency was plotted.

CHAPTER 4

RESULTS AND DISCUSSIONS

4.1 Phase formation behaviour

The phase formation behaviour was studied by XRD. The XRD patterns of the sintered $SrFe_{12}O_{19}$ hexagonal M-ferrite pellets and sintered CuO doped Strontium hexagonal M-ferrite are shown in Fig 9 and Fig 10, respectively. The phases were in crystalline state and their study revealed pure hexagonal ferrite phases similar to JCPDS card number 84-1531 and 80-1197. The metal oxide phase in the sintered pellet was absent. The lattice parameters of different ferrites are shown in Table 2.

Ref. Code	Compound Name	Chemical Formula
84-1531	Strontium Iron Oxide	$Sr\ Fe_{12}\ O_{19}$

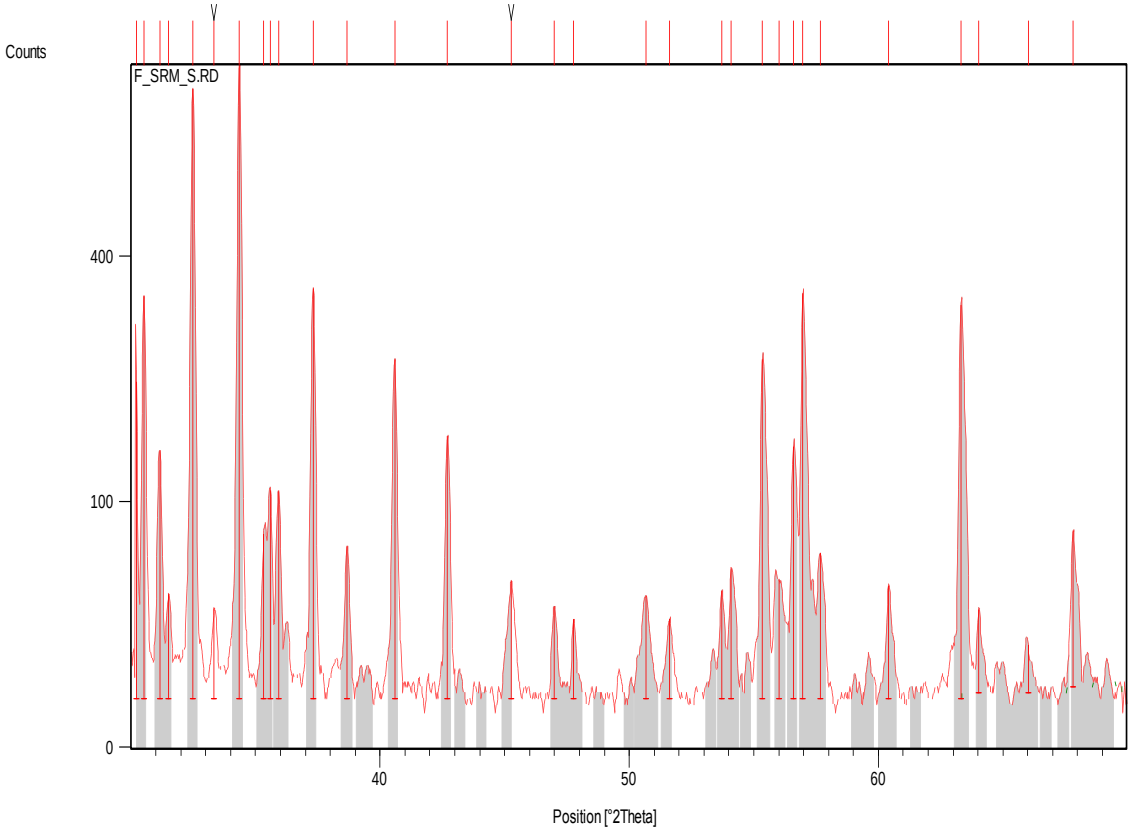

Fig. 9. XRD pattern of sintered Sr-M hexagonal ferrite

Ref. Code	Compound Name	Chemical Formula
80-1197	Strontium Iron Oxide	$Sr\ Fe_{12}\ O_{19}$

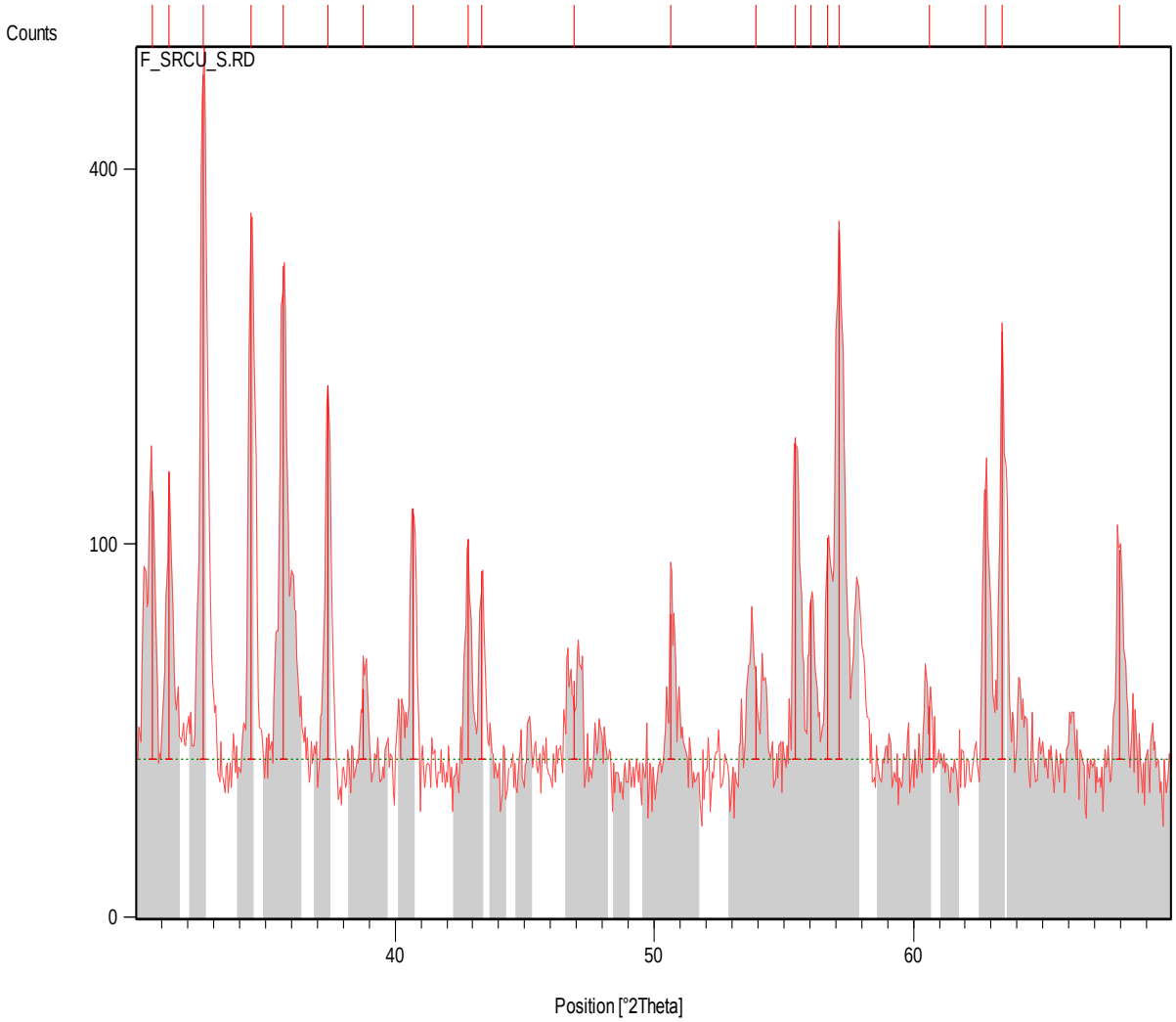

Fig. 10. XRD pattern of sintered CuO-doped ferrite.

4.2 Densification analysis

Lattice parameters of respective ferrite were calculated and they are presented in table 2. The result shows that the lattice parameter, mainly '*c*' decreases with the substitution of Zn and Ti in place of iron in the hexagonal structure. As the ionic diameter of Ti^{+4} (60.5 pico meter) and Zn^{+2} (74 pico meter) are smaller than Fe^{+3} (64.5 pico meter) and Fe^{+2} (78 pico meter) respectively, the lattice parameter 'c' decreases from 22.91 to 22.84 Å. The Bi_2O_3 and CuO doped ZnTi-SrM ferrite shows

no change in lattice parameter '*c*' compared to (Zn ,Ti) SrM ferrite. This indicates that Bi_2O_3 and CuO do not get substituted in the structure.

Table 2 Lattice parameter of different ferrites

Material	Lattice Parameter (Å) (a = b)	Lattice Parameter (Å) (c)
Sr-M	5.87	22.91
ZnTi-Sr-M	5.88	22.84
Bi-Doped	5.89	22.85
CuO-Doped	5.88	22.84

Fig. 11. shows that the rate of shrinkage for CuO doped sample is much higher than that of ZnTi and Bi_2O_3 doped sample at a lower temperature. Shrinkage starts at 920^{o}C for CuO doped sample whereas ZnTi substituted sample shows starting of shrinkage at 1140^{o}C and Bi_2O_3 doped sample has the highest temperature amongst the three which is about 1200^{o}C, therefore all these indications suggest that CuO is very effective sintering aid for the ZnTi substituted ferrite.

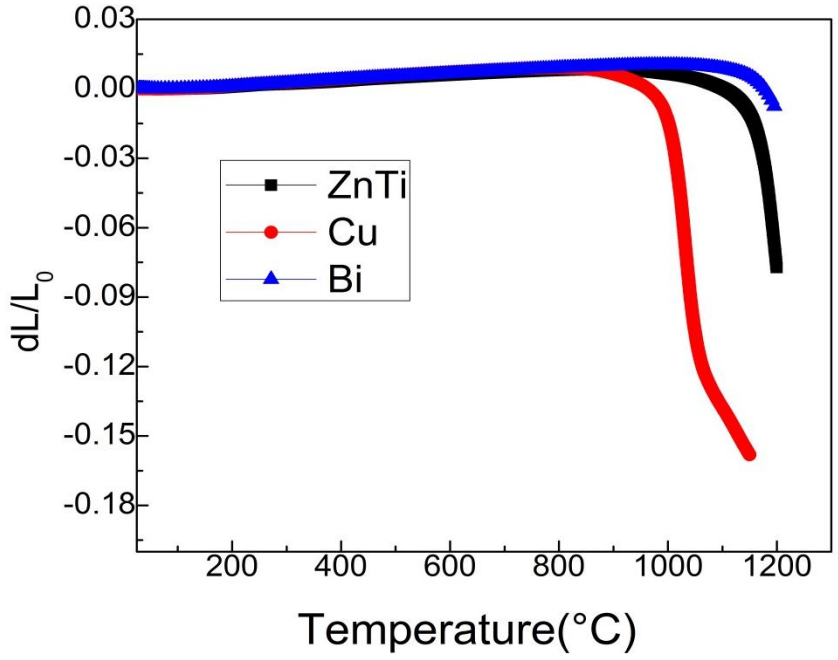

Fig. 11. Shrinkage curve at 10^{o}C/min heating rate in air for ZnTi, and CuO and Bi_2O_3 doped Strontium M-ferrite.

4.3 Microstructural analysis

Fig.12. shows the SEM microstructure of the fracture surface of different ferrites. All the ferrites show plate like hexagonal grains in their microstructure. The ZnTi substituted ferrite has well developed grains than pure SrM ferrite. Bi doped ferrite shows very small grain size due to its highest sintering temperature among all the compositions. CuO doped specimen also shows well developed hexagonal plates in its microstructure indicating that it helps in the liquid phase sintering of the ferrite where plates were grown from the liquid.

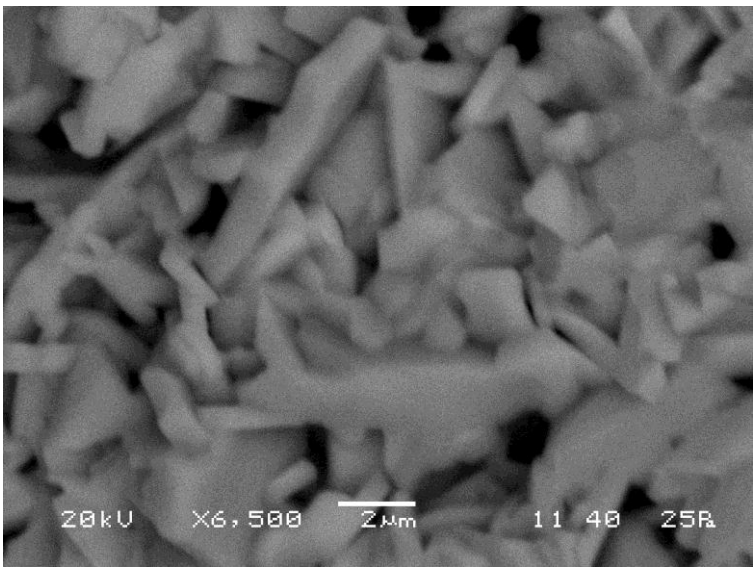

(a) Sr-M

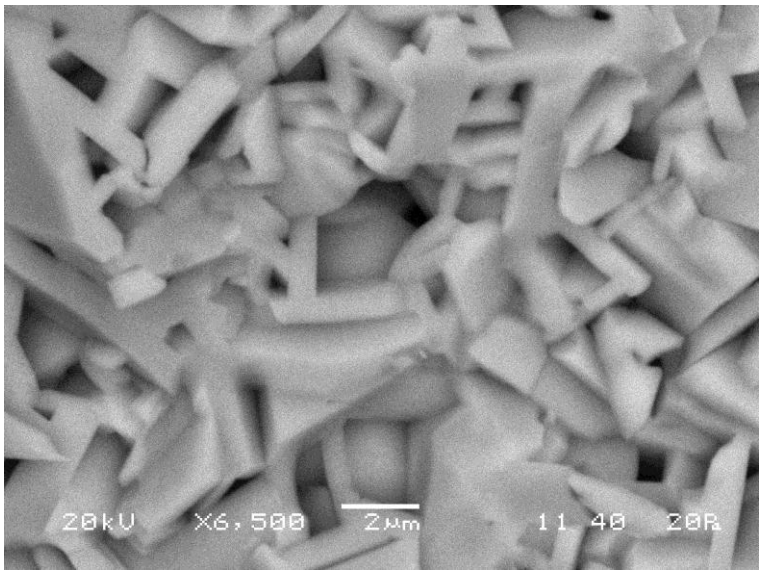

(b) Zn-Ti-substituted

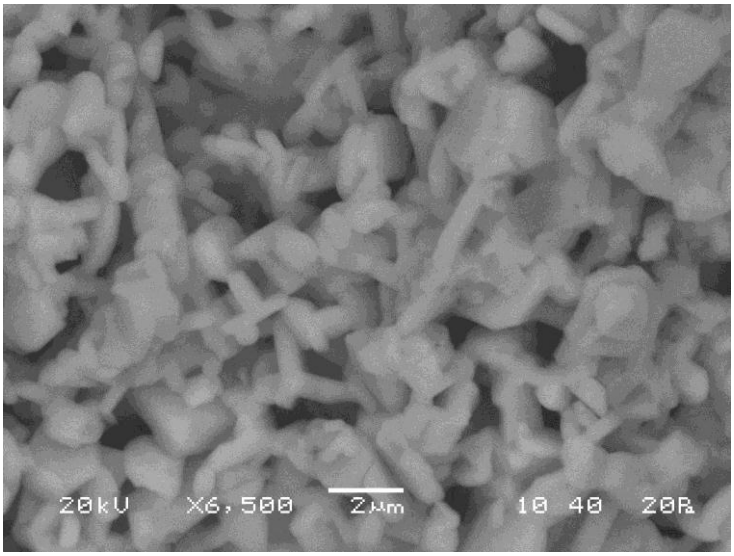

(c) Bi-doped

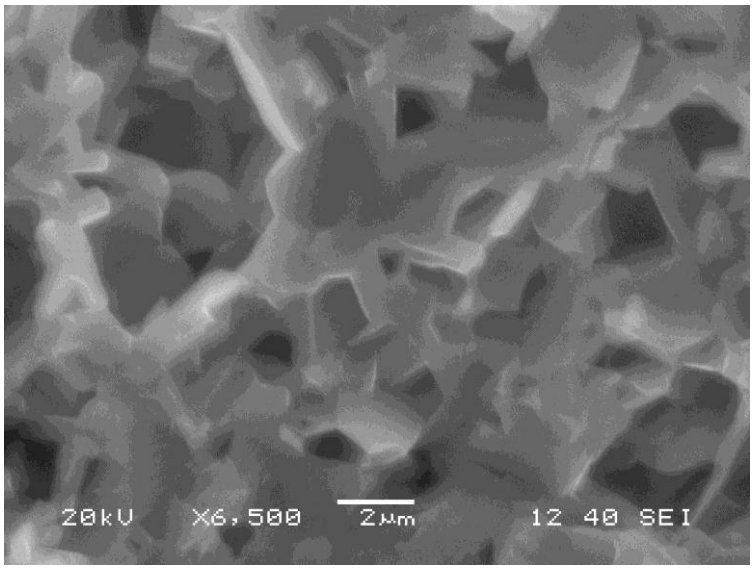

(d) **CuO-doped**

Fig.12. SEM microstructures of sintered Sr-M ferrite (a) Pure SrM, (b) ZnTi substituted Sr-M, (c) Bi-doped and (d) CuO-doped ZnTiSr-M ferrite.

4.4 Electrical properties

Fig 13. shows the frequency dependency of permittivity of SrM, ZnTi substituted SrM, Bi-doped and CuO-doped ZnTiSr-M ferrite. CuO-doped ferrite has the best permittivity, so this will be the best material among all four compositions for inductor core application. Moreover its permittivity is very stable with the change in frequency in the range of 10^3 to 10^6 Hz. Thus this CuO-doped material is suitable for a stable high frequency application in a wide frequency range.

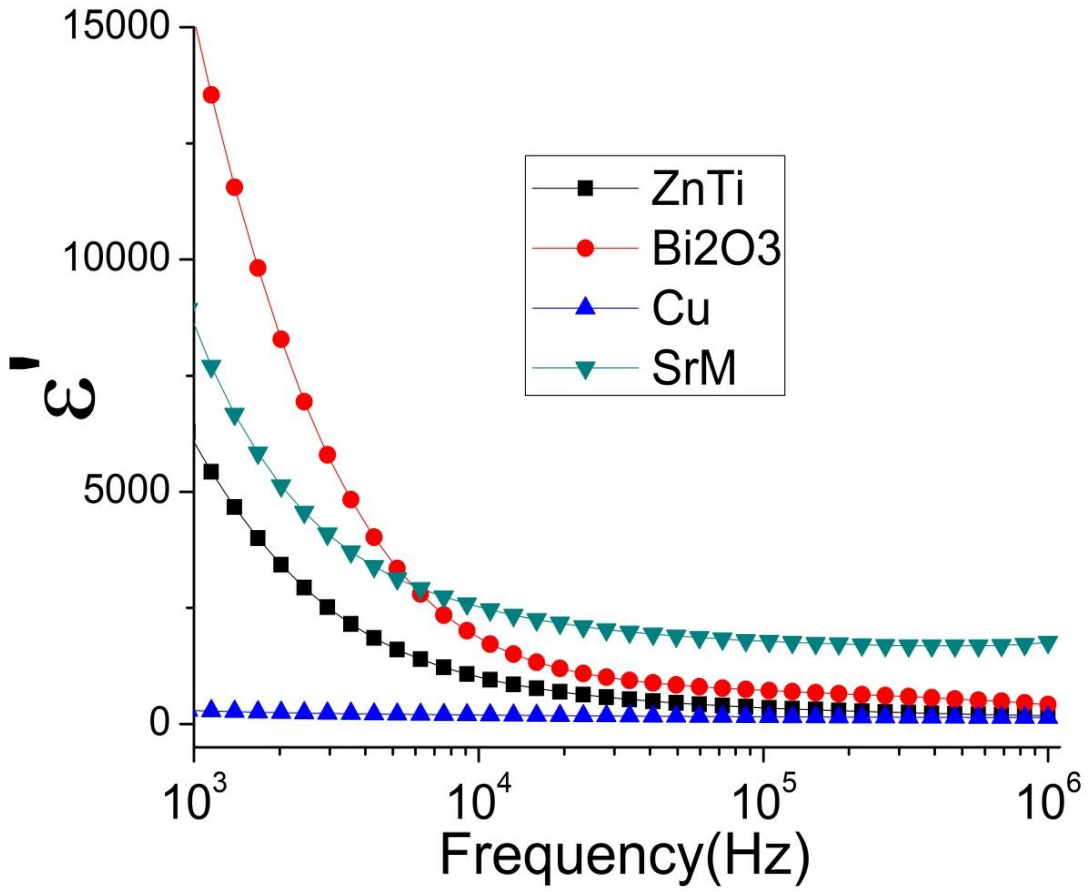

Fig. 13. Frequency dependence of permittivity for SrM, ZnTi substituted Sr-M, Bi-doped and CuO-doped ZnTiSr-M ferrite.

Fig 14. shows the frequency dependency of *tan δ* (loss factor). As expected the CuO-doped specimen has the lowest loss among all the compositions. This indicates that due to its low loss characteristics it can be used for low loss applications in high frequency inductor applications. The loss factor is a very important parameter for Multi-Layer Chip Inductor (MLCI). The *tan δ* and capacitance should be as small as possible for a good inductor material.

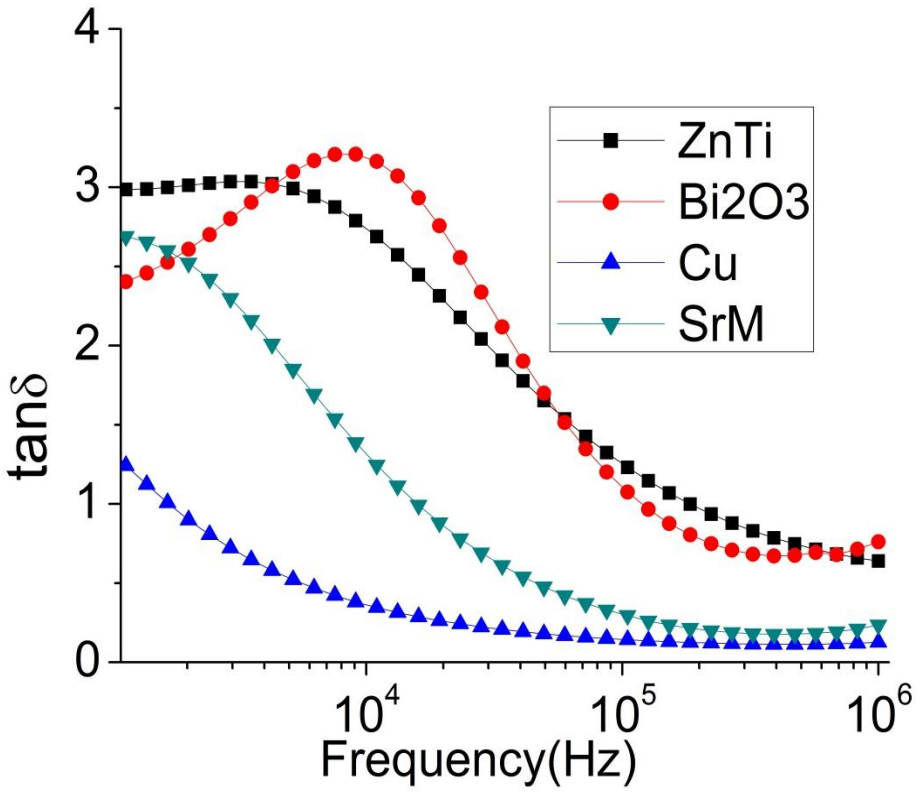

Fig. 14. Frequency dependency of Loss Factor for SrM, ZnTi substituted Sr-M, Bi-doped and CuO-doped ZnTiSr-M ferrite.

The measurement of permeability for all the compositions was done on the toroid samples. The variation of initial permeability with respect to frequency is shown in Fig 15. The CuO-doped sample shows highest value of initial permeability for a wide

range of frequency. This property makes the CuO-doped sample a suitable candidate for inductor core applications.

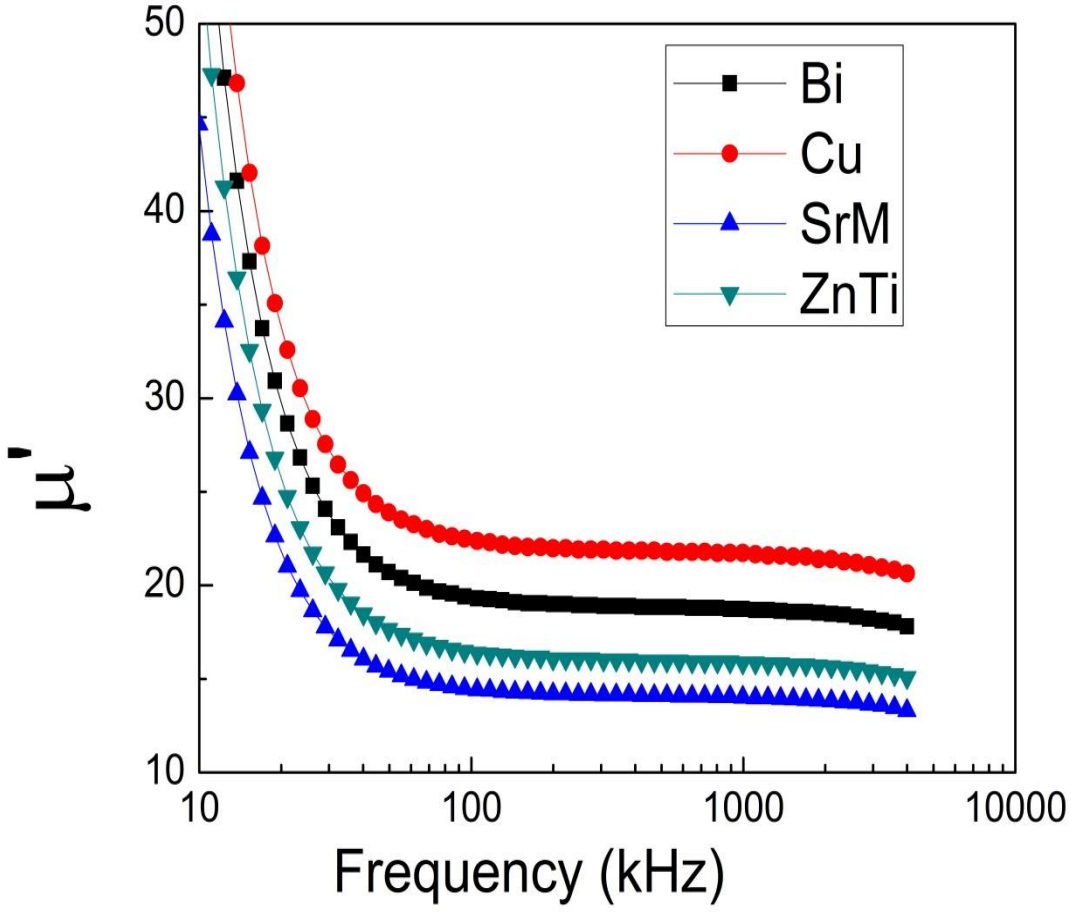

Fig. 15. Frequency dependency of initial permeability for SrM, ZnTi substituted Sr-M, Bi-doped and CuO-doped ZnTiSr-M ferrite.

The ratio of magnetic loss (tan δ) to initial permeability (μ') is also known as Relative Loss Factor (RLF). In high frequency inductor core application, a low RLF with a high μ' is required. Fig 16.shows that the RLF of CuO-doped sample is lower than all the other compositions and also that RLF decreases with increasing frequency. Thus it

can be said that CuO-doped sample is ideal for high frequency application in inductor core.

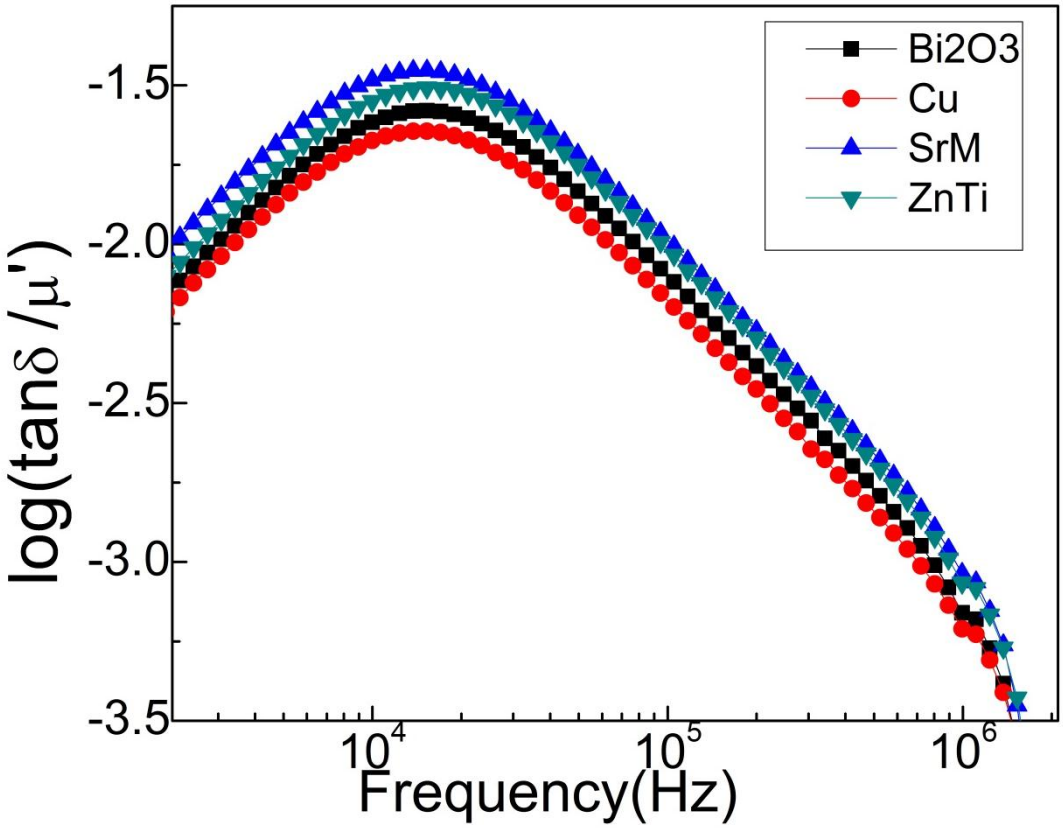

Fig. 16. Relative loss factor as a function of frequency for SrM, ZnTi substituted Sr-M, Bi-doped and CuO-doped ZnTiSr-M ferrite.

Fig 17.shows the variation of AC resistivity of all the compositions with frequency. The graph shows that CuO-doped specimen has the highest resistivity value in comparison to all the other specimens. The AC resistivity parameter is also an important parameter for ferrites in multi-layered structures. As the AC resistivity of CuO-doped sample is higher than other samples, it can be concluded that this material is better suited for high frequency inductor core application.

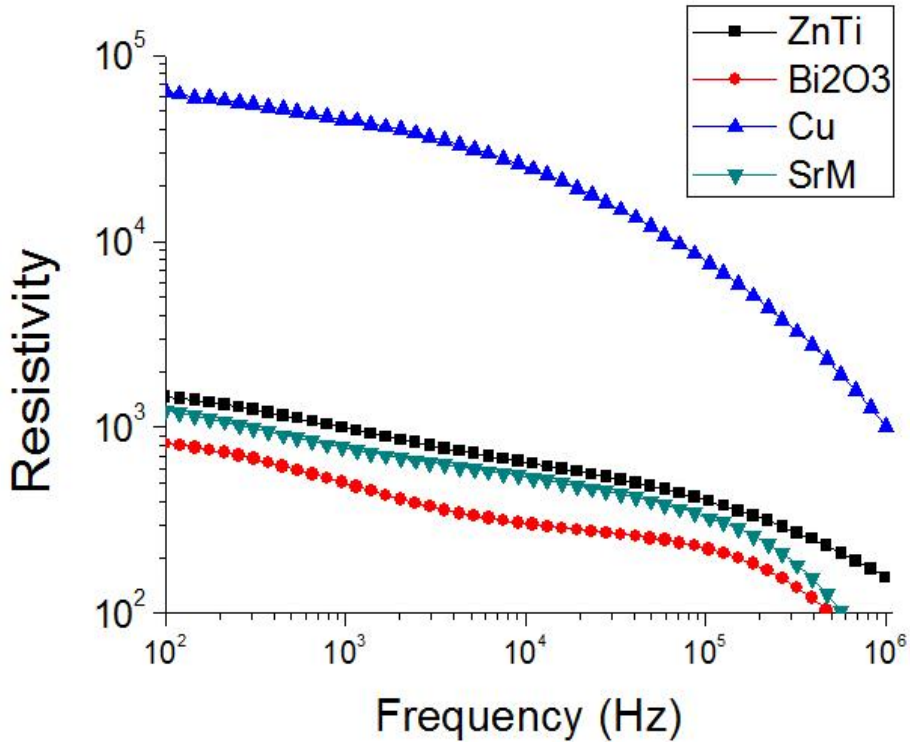

Fig. 17.AC resistivity as a function of frequency for SrM, ZnTi substituted Sr-M, Bi-doped and CuO-doped ZnTiSr-M ferrite.

Table 3 shows the permeability, permittivity, dielectric *tan δ*, *tanδ/μ'* and resistivity of all the ferrites. All the properties are found to be best in CuO-doped specimen. It has the highest permeability and lowest *tan δ* (loss factor) and highest resistivity. So this is the best material for low temperature sintered hexagonal ferrite for high frequency application.

Table 3 Permeability, permittivity, relative loss factor and resistivity of sintered Strontium M-ferrite with different doping at room temperature.

Material	Permittivity at 1 MHz	Dielectric tan δ at 1 MHz	Permeability (μ_i) at 1 MHz	$(\tan\delta)/\mu_i$ at 1 MHz	Resistivity (*$10^6\Omega$-cm) at 1 MHz
Sr-M	1760.62	0.236	13.98	0.00086	43.1
ZnTiSr-M	180.82	0.639	15.84	0.00082	156
Bi-Doped	419.96	0.761	18.67	0.00066	56.2
CuO-Doped	140.27	0.126	21.65	0.00059	1010

CHAPTER 5

CONCLUSION

Conclusion

The effect of Zn and Ti substitution along with the doping of CuO and Bi_2O_3 in $SrFe_{12}O_{19}$ has been investigated. The hexagonal M-ferrite composition was successfully synthesized by sol-gel auto-combustion method. The CuO doping of ferrite helped in better densification. The CuO-doped ferrite showed lowest dielectric permittivity and dielectric loss. Also it showed highest permeability, lowest relative loss factor and highest resistivity, respectively. The permeability was stable up to 1 MHz frequency. According to all the data presented, it can be said that CuO-doped $SrFe_{11.6}Zn_{0.2}Ti_{0.2}O_{19}$ would be a good material for multi-layer ferrite chip inductor core.

CHAPTER 6

REFERENCES

REFERENCES

[1] Smit J, Wijn HPJ. Ferrites, Philips Technical Library, Eindhoven; 1959.

[2] Robert C. Pullar, Progress in Materials Science 57 (2012) 1191–1334

[3] J. Mürbe, J. Töpfer, Journal of the European Ceramic Society 32 (2012) 1091–1098

[4] Nobuyoshi Koga, TakanoriTsutaoka, Journal of Mag and Mag Mate. 313 (2007) 168–175

[5] United States Patent Application Pub. No.: US 2012/0085963 A1, Apr.12, 2012.

[6] http://www.tdk.co.jp/techjournal_e/vol04_mlg/contents04.htm

[7] SilviaBierlich, JörgTöpfer, IEEE Transactions On Magnetics, Vol. 48, No. 4, 2012

[8] T. Tachibana, T. Nakagawa, Y. Takada, T. Shimada, and T. Yamamoto, J. Magn. Magn.Mater.vol. 284, pp. 369–375, 2004.

[9] Y. Bai, J. Zhou, Z. Gui, and L. Li, J. Magn. Magn. Mater., vol. 246, pp. 140–144, 2002.

[10] S. Bierlich,J.T¨opfer, J. Magn. Magn. Mater, 324 (2012) 1804–1808

[11] S. Krauunovská and J. Töpfer, J. Magn. Magn. Mater, vol. 320, pp. 1370–1376, 2008.

[12] Narang SB, Huidara LS. J Ceram Process Res 2006;7:113.

[13] Yamamoto H, Kumehara H, Takeuchi R, Nishio N. J Phys IV 1997;7:C1–535.

[14] Pullar RC, Taylor MD, Bhattacharya AK. J Mater Res 2001;16:3162.

[15] Jean M, Nachbaur V, Bran J, Le Breton J-M. J Alloys Compd 2010; 496:306.

[16] Sato H, Umeda T. In: Ferrites, proc ICF6, Kyoto and Tokyo; 1992. p.1122.

[17] Zhong W, Ding W, Jiang Y, Zhang N, Zhang J, Du Y, et al. J Am Ceram Soc 1997;80:3258.

[18] R. Lebourgeois, “Ferrite Material for a Permanent Magnet and Method for Production”; Patent: WO 2004/102595, PCT/EP2004/050825, May 17th 2004.

[19] DarjaLisjak and Richard Lebourgeois, J. Am. Ceram. Soc., 95 [10] 3025–3030 (2012)

[20] WandeeOnreabroy ,KomanePapato , GobwuteRujijanagul ,KamonpanPengpat , TaweeTunkasiri.Ceramics International 38S (2012) S415–S419

[21] Ali Ghasemi, Vladimir ˇSepela´k,Journal of Magnetism and Magnetic Materials 323 (2011) 1727–1733

[22] Qingqing Fang, Yanmei Liu, Ping Yin, Xiaoguang Li. Journal of Magnetism and Magnetic Materials 234 (2001) 366–370

[23] Xiansong Liu, Pablo Herna´ndez-Go´ mez, Kai Huang, Shengqiang Zhou,Yong Wang, Xia Cai, Hongjun Sun, Bao Ma. Journal of Magnetism and Magnetic Materials 305 (2006) 524–528

[24] Ali Ghasemi. Journal of Magnetism and Magnetic Materials 324 (2012) 1375–1380

[25] Kubo et. al. US patent No. 5378547

[26] Z.Yue, L. Li,J. Zhou,H. Zhang,Z. Gui, Mat. Sci. Engg. B 64 (1999) 68.

[27] M. D. Nersesyan, A. G. Peresada, A.G. Merzhanov, Int. J. SHS 7 (1998) 60.

[28] S. R. Jain, K. C. Adiga, Combustion and Flame 40 (1981)71.

[29] M.Yan, J.Hu, J. Magn. Magn. Mater. 305 (1) (2006) 171.

[30] R. C. Buchanan, Ceramic Materials for Electronics, Marcel Dekker Inc. New York, (1991) 35.